



OPEN

A machine learning based algorithm accurately stages liver disease by quantification of arteries

Zhengxin Li¹, Xin Sun², Zhimin Zhao^{2,3}, Qiang Yang⁴, Yayun Ren⁴, Xiao Teng⁵, Dean C. S. Tai⁵, Ian R. Wanless⁶, Jörn M. Schattenberg^{7,8} & Chenghai Liu^{2,3}✉

A major histologic feature of cirrhosis is the loss of liver architecture with collapse of tissue and vascular changes per unit. We developed qVessel to quantify the arterial density (AD) in liver biopsies with chronic disease of varied etiology and stage. 46 needle liver biopsy samples with chronic hepatitis B (CHB), 48 with primary biliary cholangitis (PBC) and 43 with metabolic dysfunction-associated steatotic liver disease (MASLD) were collected at the Shuguang Hospital. The METAVIR system was used to assess stage. The second harmonic generation (SHG)/two-photon images were generated from unstained slides. Collagen proportionate area (CPA) using SHG. AD was counted using qVessel (previously trained on manually labeled vessels by stained slides (CD34/a-SMA/CK19) and developed by a decision tree algorithm). As liver fibrosis progressed from F1 to F4, we observed that both AD and CPA gradually increases among the three etiologies ($P < 0.05$). However, at each stage of liver fibrosis, there was no significant difference in AD or CPA between CHB and PBC compared to MASLD ($P > 0.05$). AD and CPA performed similar diagnostic efficacy in liver cirrhosis ($P > 0.05$). Using the qVessel algorithm, we discovered a significant correlation between AD, CPA and METAVIR stages in all three etiologies. This suggests that AD could underpin a novel staging system.

Keywords Machine learning, Arterial density, Liver fibrosis, Chronic liver disease.

Cirrhosis is the end stage of chronic liver diseases (CLDs) arising from various etiologies. Clinically, liver biopsies and non-invasive tests assist in determining the fibrosis stages of CLDs. While non-invasive tests are increasingly available¹, only liver histology does allow to assess morphological features of CLDs. However, relying solely on collagen degradation may limit our understanding of CLDs staging, as fibrosis does not fully encompass the complexity of biological events that occur as CLDs progress². A more comprehensive histological assessment ought to consider factors affecting the disease's progression or regression³.

Vascular changes are a critical factor that has garnered considerable attention in the context of progressing or regressing liver fibrosis⁴. Previous studies have demonstrated that arterial and ductal densities correlate with the histologic stages as defined by the METAVIR, Ishak, or Laennec systems^{5,6}. Hepatic vascular alterations facilitate the progression of CLDs by disrupting the liver's internal homeostasis⁷. Improving vascular changes by protecting endothelial cells can inhibit the liver fibrosis, as evidenced by the use of anticoagulants, simvastatin, and vascular endothelial growth factor (VEGF) modulation^{8–13}. Notably, distinct vascular features aid the regression of CLDs by reducing tissue hyperemia^{7,14}. The significance of vascular changes on the progression and regression of liver fibrosis is clear, yet the distinct differences in these changes across various CLDs etiologies remain undefined.

Among existing digital methods for analyzing vessels, microvessel density (MVD) is often used as a surrogate marker for assessing angiogenesis¹⁵. Whole-slide scanning and algorithm-based uniform random sampling are employed to minimize sampling errors¹⁶. However, traditional MVD metrics cannot differentiate between arteries and veins. The limitations of liver histology in assessing fibrosis stages are multifaceted^{17,18}.

Imaging modalities like magnetic resonance imaging (MRI) and computed tomography (CT) are employed to directly observe blood vessels and bile ducts, while magnetic resonance angiography (MRA) necessitates contrast agents¹⁹. In contrast, MRA may be augmented with specific antigens, antibodies, or small molecule fluorescent probes to enhance contrast based on the requirements of scientific research, enabling precise

¹Gongli Hospital of Shanghai Pudong New Area, Shanghai, China. ²Shuguang Hospital, Shanghai University of Traditional Chinese Medicine, 528 Zhangheng Road, Pudong New Area, Shanghai 201203, China. ³Shanghai Key Laboratory of Traditional Chinese Clinical Medicine, Shanghai, China. ⁴Hangzhou Choutu Tech. Co., Ltd., Hangzhou, China. ⁵Histoindex Pte. Ltd, Singapore, Singapore. ⁶Department of Pathology, Queen Elizabeth II Health Sciences Centre, Dalhousie University, Halifax, Canada. ⁷Department of Internal Medicine II, Saarland University Medical Center, Homburg, Germany. ⁸Saarland University, Saarbrücken, Germany. ✉email: chenghai.liu@outlook.com

Stage(n)	CHB (N=46)	PBC (n=48)	NAFLD (n=43)	P
F1	7	8	5	0.755
F2	11	15	8	
F3	12	12	12	
F4	16	13	18	

Table 1. Basic information of chronic hepatitis patients due to CHB/PBC/NAFLD.

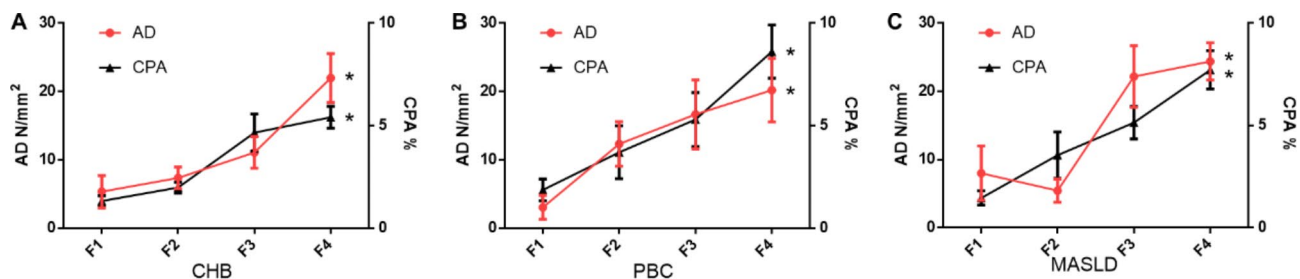


Fig. 1. Changes of AD and CPA in different stages of CLDs.

localization²⁰. Yet, given the limits of imaging principles, visualizing microvasculature smaller than 100 μm remains challenging, impeding both widespread application and research efforts.

Machine learning technologies have become increasingly integral in medical research in recent years. For instance, qFibrosis²¹, founded on second harmonic generation/two-photon (SHG-TP) fluorescence microscopy, offers a stable, repeatable, and visual quantitative method for quantitatively assessing liver fibrosis in CLDs, and which exhibiting high correlation with METAVIR fibrosis scores^{21,22}. Our research introduces a qualitative and quantitative approach (qVessel) based on SHG-TP. This method evaluates changes in microvessel structure across different chronic liver diseases with visible detail. We anticipate that it will significantly enhance the pathological understanding and assist in the regression of liver cirrhosis.

Results

Clinical information

This study included 46 patients with chronic hepatitis B (CHB), comprising 25 males and 21 females, ranging in age from 32 to 65 years. The distribution of patients across METAVIR fibrosis stages was as follows: 7 patients in the F1 stage, 11 in F2, 12 in F3, and 16 in F4. Additionally, the study enrolled 48 patients with primary biliary cholangitis (PBC), including 22 males and 26 females, aged between 33 and 67 years. The breakdown by fibrosis stage for PBC patients was 8 in F1, 15 in F2, 12 in F3, and 13 in F4. The cohort also included 43 patients with metabolic dysfunction-associated steatotic liver disease (MASLD), consisting of 8 males and 35 females aged from 23 to 69 years. The number of MASLD patients at each fibrosis stage was 5 at F1, 8 at F2, 12 at F3, and 18 at F4 (see Table 1 for details).

Arterial recognition results of qVessel

The cross validation showed the qVessel algorithm's average overall True Positive Rate (TPR) was 0.38, and the True Negative Rate (TNR) was 0.90. Conversely, the False Positive Rate (FPR) stands at 0.10, and the False Negative Rate (FNR) was 0.62. Detailed recognition parameters for each sample were presented in Supplement Table 1. The average repeatability consistency of the qVessel algorithm for the rotated images was 75.85% (Supplement Table 2).

Arterial density (AD) and collagen proportionate area (CPA) increased with progressing liver fibrosis stages

As liver fibrosis progressed from F1 to F4, AD showed positive correlation with fibrosis stages of the three etiologies ($P < 0.05$) (Fig. 1). The r value of CHB, PBC and MASLD are 0.530 ($P = 0.000$), 0.470 ($P = 0.001$), 0.612 ($P = 0.000$), respectively. However, no significant differences were found between the different etiologies within each fibrosis stage ($P > 0.05$) (Table 2).

Similarly, with progressing liver fibrosis stages (F1 to F4), CPA of the three etiologies also showed positive correlation with fibrosis stages ($P < 0.05$) (Fig. 1). The r value of CHB, PBC and MASLD are 0.754 ($P = 0.000$), 0.674 ($P = 0.001$), 0.612 ($P = 0.000$), respectively. Yet, there were no significant differences noted between different etiologies within each stage ($P > 0.05$) (Fig. 1; Table 3).

AD and CPA performed similar diagnostic efficacy in liver cirrhosis

The area under the receiver operating characteristic curve (AUROC) of AD for diagnosing F4 was 0.804 (95% CI, 0.661–0.947; $P = 0.001$; sensitivity, 81.3%; specificity, 76.7%) in CHB, 0.699 (95% CI, 0.550–0.848; $P = 0.036$;

Stage	NAFLD	CHB	P	PBC	P
F1	5.08 (0.00,17.46)	4.08 (0.16,8.96)	0.679	0.96 (0.00,,5.94)	0.452
F2	5.11 (0.52,9.29)	7.50 (3.16,11.86)	0.455	8.59 (2.58,21.54)	0.194
F3	15.33 (8.47,35.21)	10.49 (6.28,16.34)	0.092	11.47 (4.67,22.35)	0.144
F4	21.72 (15.87,27.32)	19.91 (12.44,29.31)	0.572	16.25 (8.73,26.55)	0.096

Table 2. Comparisons between AD in different stages of CLDs.

Stage	NAFLD	CHB	P	PBC	P
F1	1.45 ± 0.78	1.33 ± 0.68	0.760	1.87 ± 1.49	0.434
F2	3.54 ± 3.39	1.98 ± 0.87	0.000	2.80 ± 3.64	0.476
F3	5.13 ± 2.86	4.66 ± 3.15	0.702	4.09 ± 2.05	0.319
F4	7.71 ± 3.97	5.41 ± 2.12	0.097	7.87 ± 4.13	0.660

Table 3. Comparisons between CPA in different stages of CLDs.

	CPA	AD	P
CHB	0.848 (0.734,0.962)	0.804 (0.661,0.947)	0.637
PBC	0.873 (0.772,0.974)	0.699 (0.550,0.848)	0.059
NAFLD	0.788 (0.654,0.923)	0.776 (0.633,0.920)	0.905

Table 4. Comparison of AUROCs between CPA and AD in different CLDs.

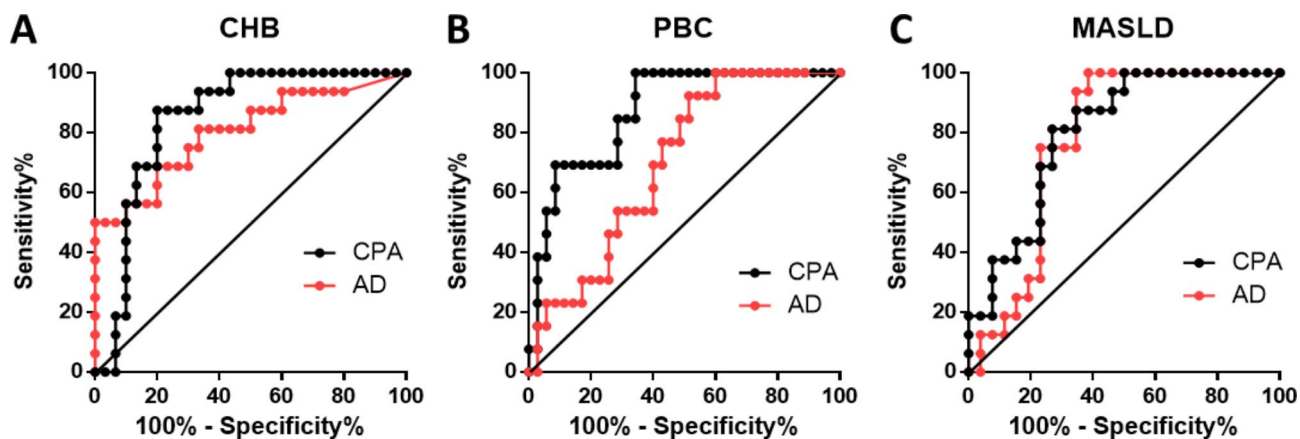


Fig. 2. AUROC of AD and CPA in diagnosing F4 of CLDs.

sensitivity, 92.3%; specificity, 48.6%) in PBC, and 0.776 (95% CI, 0.633–0.920; $P=0.003$; sensitivity, 100.0%; specificity, 61.5%) in MASLD.

The AUROC of CPA for diagnosing F4 was 0.848 (95% CI, 0.734–0.962; $P=0.000$; sensitivity, 87.5%; specificity, 80.0%) in CHB, 0.873 (95% CI, 0.772–0.974; $P=0.000$; sensitivity, 100.0%; specificity, 65.7%) in PBC, and 0.788 (95% CI, 0.654–0.923; $P=0.002$; sensitivity, 81.3%; specificity, 69.2%) in MASLD.

There was no significant difference between AD and CPA for diagnosing F4 in CHB ($P>0.05$), MASLD ($P>0.05$), and PBC ($P=0.059$). (Table 4; Fig. 2)

Discussion

Assessing liver fibrosis is an effective means to estimate the progression and prognosis of CLDs, to determine the optimal treatment timing, to monitor drug efficacy, and to guide long-term management²³. Non-invasive tests (NITs) have been regarded as an ideal indicator for evaluating liver fibrosis, which has good reproducibility and is easy to promote. It mainly includes direct serum markers, composite serum marker diagnostic models, and imaging methods. However, there are no exact serum markers or composite models reported to predict fibrosis regression. Liver stiffness measurement (LSM) which is currently the most well-known transient elastography. Although LSM has certain advantages in the diagnosis of advanced liver fibrosis in CLDs²⁴, its value of drug

efficacy evaluation for liver fibrosis has not been widely recognized. Previous randomized controlled trials have shown that the changes of LSM were only a predictor for the regression of inflammation rather than liver fibrosis^{25,26}. The clinical guidelines suggested that the higher LSM, the higher the sensitivity and specificity for liver fibrosis. Given that higher LSM have a wider range of potential for decline, it is more likely to achieve positive conclusions in cirrhosis patients. Therefore, liver biopsies are still the best method for evaluating the stage and drug efficacy of liver fibrosis.

To the best of our knowledge, this study is the first to show arterial changes across various etiologies of CLDs using a non-staining, quantitative methodology. It has been traditionally thought that changes in vascular structure are mostly observed in cirrhosis or advanced stages of fibrosis. Nevertheless, our research indicates that these alterations can also occur in the early to intermediate stages of fibrosis, and that vascular changes differ among the different etiologies of CLDs.

The SHG/TP imaging system was first described and invented by Tai et al.²⁷. Over time, this methodology has evolved and is now extensively applied in the clinical research of liver diseases, allowing for the quantitative analysis of both the quantity and structure of collagen²¹. Compared to conventional histopathological assessments, this approach can more accurately capture the regression trends in hepatitis B-related fibrosis^{28,29} and can provide stable and precise evaluations for small liver biopsy specimens that are challenging to assess through traditional pathology³⁰. As such, it considerably reduces inter-observer variability stemming from manual assessments and the inconsistencies between different evaluation systems, such as reconciling between the Ishak and METAVIR fibrosis scoring systems³¹. Building on this foundation, qVessel expands the capabilities to differentiate and quantify vessels, aiming to digitally visualize liver pathology. This provides a means for quantitative and qualitative comparisons between diseases and offers an objective basis for more refined staging and pharmacodynamic evaluations of liver fibrosis.

The chronic course of liver fibrosis is a struggle between liver inflammation and regeneration, and liver inflammation which is known as parenchymal extinction (PE) is closely related to fibrosis stages. In a normal liver, the portal stroma and sinusoidal reticulin fibers constitute the main types of collagen. During PE, the stroma collapses and collagen concentration can increase from 4% to as much as 50%, with a concomitant decrease in collagen synthesis⁵. As such, PE is considered a principal factor contributing to the elevated collagen concentration seen in cirrhosis⁶. This concept has been supported by findings in acute fulminant liver failure³². Based on the concepts, we evaluate the fibrosis stages by observing the morphology and quantity of fibers^{33–35}. However, vascular heterogeneity is also an important characteristic in liver fibrosis³⁶. For example, chronic inflammation in the portal tract is characterized not only by fibrotic collagen deposition but also by varying degrees of edema and inflammation of the vascular endothelium, which in severe cases can lead to portal vein thrombosis and occlusion^{37–39}. Following early obstruction of small portal veins, portal vein flow becomes relatively insignificant, making hepatic artery flow a useful proxy for inflow load in the sinusoids. With the occurrence of PE, the arteries persist to supply the remaining parenchymal cells. Therefore, AD has been suggested as an indicator of PE. Our research shows that AD displays a strong correlation with CPA and the METAVIR staging system, and both should be considered simultaneously when determining the stages of fibrosis.

Liver injury will stimulate the wound healing response, and rapid cell proliferation requires a large amount of blood flow and nutrient supply, leading to local hypoxia in liver tissue. Under the involvement of hypoxia inducible factor-1 (HIF-1), tissue hypoxia stimulates hepatocytes to upregulate the expression of VEGF, angiopoietin I (Ang I), and related receptors⁴⁰, thereby inducing angiogenesis and promoting the increase of AD. Meanwhile, other cytokines that have dual effects of promoting fibrosis and angiogenesis, such as platelet growth factor, transforming growth factor- β , fibroblast growth factor, continuously promote the formation of PE through autocrine and paracrine pathways of activated hepatic stellate cells and sinusoidal endothelial cells, ultimately leading to cirrhosis⁴¹. The destruction of liver lobules, alteration in tissue blood oxygen concentration, and relative immunosuppression caused by heterogeneous oxygen distribution collectively create a conducive internal environment for tumor development⁴².

In advanced fibrosis, the increasing of AD in MASLD is greater than that in CHB and PBC, which is consistent with previous reported. The proliferation of artery in the central vein area could be observed in the early stage of MASLD⁴³. The abnormal changes in vessels may be the vascular basis for the occurrence of hepatocellular carcinoma in non-cirrhotic MASLD compared to other CLDs. The reason for this may be related to the histological feature of chicken-wire fibrosis in MASLD. The formation of peri cellular fibrosis completely isolates the exchange of substances between hepatocytes and sinusoids, and the pathological changes of cell apoptosis are more easily observed (ballooning and Mallory bodies). Ischemia and hypoxia stimulate the synthesis and release of VEGF, Ang, endothelin, and nitric oxide, thereby promoting angiogenesis. Although CHB and PBC share similar molecular mechanisms, the fibrosis is more pronounced in the portal area, and the abundant blood flow crossing in the hepatic sinusoids partially alleviates the differences in blood oxygen distribution caused by ischemia and hypoxia.

The three causes of CLDs represent portal tract expansion in post-necrotic fibrosis, biliary fibrosis and pericentral fibrosis respectively⁴⁴. The different fibrosis types may be the main reason for the differences in AUROC of CPA. The differences in AUROC of AD may be related to the different intrahepatic pressure. The physiological structure of liver lobules involves a pressure balance between the fluid inflow and outflow. There is vascular obstruction and local hyperemia that causes a departure from this range, summarized as “in-out-imbalance”(IOI)⁷. The obstruction of bile flow caused by cholangitis can also induce IOI, thereby limiting the compensation of angiogenesis for hypoxia. This may be the reason for the poor diagnostic efficacy of AD in biliary fibrosis.

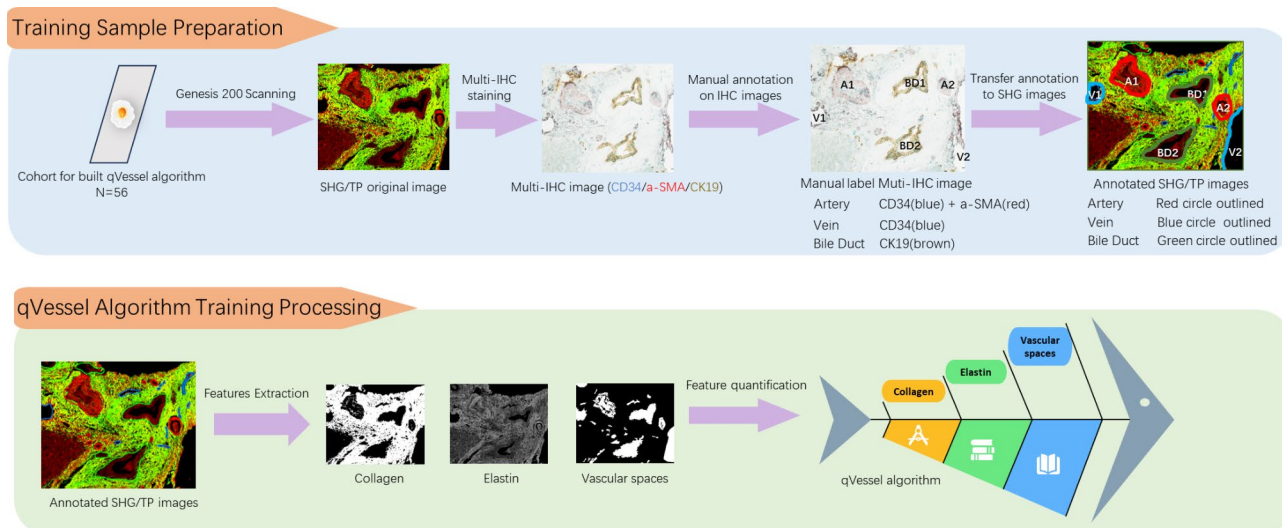


Fig. 3. Flowchart of qVessel.

Limitations

Our study is limited by the simple sizes; hence, the sample sizes for various diseases are restricted, and sampling error is inherent. Our data is based on self-validation algorithms, new samples are still needed to modify the algorithm and make it more realistic. Since all samples are derived from humans, the qVessel algorithm may not be directly applicable to pharmacodynamic evaluations in animal models, potentially limiting its broader application. Current technological constraints mean that qVessel does not account for the number of vessels in the hepatic sinusoids when quantifying blood vessels. A future objective is to overcome this limitation.

Conclusions

In conclusion, qVessel is a quantitative and qualitative visualization algorithm for liver vessels, which employs a synergistic approach of classical pathology and artificial intelligence. The microvascular alterations it uncovers contribute to a deeper understanding of the pathogenesis and evolution of liver fibrosis, aiding in the refinement of fibrosis staging and in the assessment of clinical drug efficacy.

Methods

Patients

All patients were recruited from January 2010 to December 2023 at Shuguang Hospital. The study collected 46 needle biopsies from patients with CHB, 48 from those with PBC, and 43 from individuals with MASLD. (Approval Number:2015-445-73-01, Institutional Review Board of Shuguang Hospital)

Each liver biopsy specimen was acquired using a 16-gauge needle through transcutaneous biopsy, ensuring a tissue length greater than 1.5 cm. The specimens were then formalin-fixed and paraffin-embedded (FFPE) for preservation.

Histological assessment

The METAVIR staging system was employed to evaluate fibrosis stages on trichrome-stained tissues. An experienced liver histopathologist (Dr. Kun Liu; Pathology Department of Shuguang Hospital).

For SHG-TP, unstained slides of all samples ($n = 137$) were analyzed on identical equipment (Genesis system; HistoIndex Pte., Singapore) as described previously^{27–30}. CPA is measured by using SHG⁴⁵.

Multi-immunohistochemical (Multi-IHC) staining

The sequential immunohistochemistry consisting of iterative cycles of staining, scanning, and antibody/chromogen stripping was performed according to a modified protocol based on previous reports^{46,47}. The slides were visualized with either an anti-mouse or anti-rabbit horseradish peroxidase-conjugated polymer (ab236467, Abcam), followed by peroxidase detection with 3,3'-Diaminobenzidine Tetrahydrochloride (DAB) for CK19(ab52625,1:200, Abcam), 3-Amino-9-Ethylcarbazole (AEC) for a-SMA (ab5694,1:200, Abcam), and Emerald for CD34(ab81289,1:50, Abcam).

Development of qVessel algorithm

The qVessel algorithm was a machine learning-based method for identification of arteries from SHG/TP images (Fig. 3). 56 biopsy samples (23 CHB patients, 19 PBC patients and 14 MASLD patients) with different etiologies and fibrosis stages were randomly selected as the training cohort of qVessel algorithm. After collecting SHG/TP original images of the training cohort, Multi-IHC staining was performed for the same samples. The Multi-IHC images were collected by a digital pathology slide scanner (scn400, LEICA company, Germany). In the Multi-

IHC images, Veins were revealed in blue by CD34, bile ducts were revealed in brown by CK19, and arteries were revealed in red by SMA. The locations of veins, bile ducts and arteries were annotated from the Multi-IHC images by a pathologist. The pathologist's annotations were used as the ground truth for the training of qVessel algorithm.

As described in the previous study⁴⁵, collagen and liver tissue regions were detected from the SHG channel and TP channel, respectively, using the Otsu's automatic threshold method⁴⁸. All lumen candidates including veins, arteries, bile ducts, fat vacuoles, sinusoids and cracks were identified within the liver tissue region. To differentiate arteries from other lumens, multiple pathological features for the lumen candidates were defined and measured, such as the brightness of lumen wall, the length and width of lumens, the morphological characteristics of collagen fiber and elastin signal surrounding the lumen candidates. Then, we trained a decision tree model for artery classification based on the ground truth and the features of lumen candidates, using the classification and regression tree (CART) method⁴⁹. qVessel algorithm can measure the AD which was the number of arteries per 1 mm² tissue area.

To estimate how accurately the model will perform in practice, leave-one-out cross-validation method was used. Briefly, one sample is randomly retained as the validation data while the remaining 55 samples are used as training data to construct the model. The cross-validation process is repeated 56 times, with a different sample left out each time. The overall performance of the model is assessed based on the TPR, TNR, FPR and FNR.

During the process of repeatability test, 19 samples were randomly selected and rotated 90° to evaluate the robustness of qVessel algorithm. The same arteries identified from both raw and rotated images by the algorithm were counted and analyzed for the repeatability test (Supplements results).

Statistical analysis

Data analysis was conducted using SPSS 22.0 software. Measurement data were presented as mean ± standard deviation. Categorical data were described using frequencies, and comparisons were made using the χ^2 (chi-square) test. One-way ANOVA was utilized in comparisons of CPA between MASLD and CHB or PBC, respectively. Wilcoxon rank-sum test was used for comparisons of AD between MASLD and CHB or PBC, respectively. The AUROC were used to assess the diagnostic accuracy of CPA and AD for liver cirrhosis, the cut-off value was used Youden Index, 95% confidence interval (95% CI), and sensitivity/specificity approaches to describe the outcomes. Delong test was used to compare AUROC. Statistical significance was established at a two-tailed P-value of less than 0.05 ($P < 0.05$).

Data availability

The datasets used and/or analysed during the current study available from the corresponding author on reasonable request.

Received: 6 May 2024; Accepted: 20 January 2025

Published online: 24 January 2025

References

- Armandi, A. et al. Emerging concepts in the detection of liver fibrosis in non-alcoholic fatty liver disease. *Expert Rev. Mol. Diagn.* **23**, 771–782. <https://doi.org/10.1080/14737159.2023.2242779> (2023).
- Rosselli, M., MacNaughtan, J., Jalan, R. & Pinzani, M. Beyond scoring: a modern interpretation of disease progression in chronic liver disease. *Gut* **62**, 1234–1241. <https://doi.org/10.1136/gutjnl-2012-302826> (2013).
- Guido, M. et al. Focus on histological abnormalities of intrahepatic vasculature in chronic viral hepatitis. *Liver Int.* **38**, 1770–1776. <https://doi.org/10.1111/liv.13718> (2018).
- Wang, D. et al. Angiogenesis—an emerging role in organ fibrosis. *Int. J. Mol. Sci.* **24** <https://doi.org/10.3390/ijms241814123> (2023).
- Wanless, I. R. et al. THU-101-artery density in human liver: a valuable measure for staging of chronic liver disease. *J. Hepatol.* **70**, e205 [https://doi.org/10.1016/S0618-8278\(19\)30382-2](https://doi.org/10.1016/S0618-8278(19)30382-2) (2019).
- Wanless, I. R. et al. Importance of tissue collapse and unmasking of reticulin on the assessment of fibrosis in acute and chronic liver disease. *Hepatology* **64**, 214A. <https://doi.org/10.1002/hep.28797> (2016).
- Wanless, I. R. The role of vascular injury and congestion in the pathogenesis of cirrhosis: the congestive escalator and the parenchymal extinction sequence. *Curr. Hepatol. Rep.* **19**, 40–53. <https://doi.org/10.1007/s11901-020-00508-y> (2020).
- Yang, L. et al. Vascular endothelial growth factor promotes fibrosis resolution and repair in mice. *Gastroenterology* **146**, 1339–1350.e1331. <https://doi.org/10.1053/j.gastro.2014.01.061> (2014).
- Villa, E. et al. Enoxaparin prevents portal vein thrombosis and liver decompensation in patients with advanced cirrhosis. *Gastroenterology* **143**, 1253–1260.e1254. <https://doi.org/10.1053/j.gastro.2012.07.018> (2012).
- Schepis, F. & Villa, E. Thrombophilic genetic risk factors for liver fibrosis: to screen or not to screen? *J. Hepatol.* **63**, 1311–1313. <https://doi.org/10.1016/j.jhep.2015.09.018> (2015).
- Tripathi, D. M. et al. Simvastatin prevents progression of acute on chronic liver failure in rats with cirrhosis and portal hypertension. *Gastroenterology* **155**, 1564–1577. <https://doi.org/10.1053/j.gastro.2018.07.022> (2018).
- Meireles, C. Z. et al. Simvastatin attenuates liver injury in rodents with biliary cirrhosis submitted to hemorrhage/resuscitation. *Shock* **47**, 370–377. <https://doi.org/10.1097/shk.0000000000000734> (2017).
- Turco, L. et al. Lowering portal pressure improves outcomes of patients with cirrhosis, with or without ascites: a meta-analysis. *Clin. Gastroenterol. Hepatol.* **18**, 313–327.e316. <https://doi.org/10.1016/j.cgh.2019.05.050> (2020).
- Stueck, A. E. & Wanless, I. R. Hepatocyte buds derived from progenitor cells repopulate regions of parenchymal extinction in human cirrhosis. *Hepatology* **61**, 1696–1707. <https://doi.org/10.1002/hep.27706> (2015).
- Nowak-Sliwiska, P. et al. Consensus guidelines for the use and interpretation of angiogenesis assays. *Angiogenesis* **21**, 425–532. <https://doi.org/10.1007/s10456-018-9613-x> (2018).
- Marien, K. M. et al. Development and validation of a histological method to measure microvessel density in whole-slide images of cancer tissue. *PLoS One*. **11**, e0161496. <https://doi.org/10.1371/journal.pone.0161496> (2016).
- Schattenberg, J. M. & Straub, B. K. On the value and limitations of liver histology in assessing non-alcoholic steatohepatitis. *J. Hepatol.* **73**, 1592–1593. <https://doi.org/10.1016/j.jhep.2020.07.020> (2020).
- Labenz, C. et al. Predictors of advanced fibrosis in non-cirrhotic non-alcoholic fatty liver disease in Germany. *Aliment. Pharmacol. Ther.* **48**, 1109–1116. <https://doi.org/10.1111/apt.14976> (2018).

19. Liu, Y. et al. Gadolinium-loaded polymeric nanoparticles modified with Anti-VEGF as multifunctional MRI contrast agents for the diagnosis of liver cancer. *Biomaterials* **32**, 5167–5176. <https://doi.org/10.1016/j.biomaterials.2011.03.077> (2011).
20. Cyran, C. C. et al. Permeability to macromolecular contrast media quantified by dynamic MRI correlates with tumor tissue assays of vascular endothelial growth factor (VEGF). *Eur. J. Radiol.* **81**, 891–896. <https://doi.org/10.1016/j.ejrad.2011.07.016> (2012).
21. Xu, S. et al. qFibrosis: a fully-quantitative innovative method incorporating histological features to facilitate accurate fibrosis scoring in animal model and chronic hepatitis B patients. *J. Hepatol.* **61**, 260–269. <https://doi.org/10.1016/j.jhep.2014.02.015> (2014).
22. Wang, T. H., Chen, T. C., Teng, X., Liang, K. H. & Yeh, C. T. Automated biphasic morphological assessment of hepatitis B-related liver fibrosis using second harmonic generation microscopy. *Sci. Rep.* **5**, 12962. <https://doi.org/10.1038/srep12962> (2015).
23. de Franchis, R. Expanding consensus in portal hypertension: report of the Baveno VI Consensus Workshop: stratifying risk and individualizing care for portal hypertension. *J. Hepatol.* **63**, 743–752. <https://doi.org/10.1016/j.jhep.2015.05.022> (2015).
24. Chen, Y. P., Peng, J. & Hou, J. L. Non-invasive assessment of liver fibrosis in patients with chronic hepatitis B. *Hepatol. Int.* **7**, 356–368. <https://doi.org/10.1007/s12072-013-9439-y> (2013).
25. Dong, X. Q., Wu, Z., Li, J., Wang, G. Q. & Zhao, H. Declining in liver stiffness cannot indicate fibrosis regression in patients with chronic hepatitis B: a 78-week prospective study. *J. Gastroenterol. Hepatol.* **34**, 755–763. <https://doi.org/10.1111/jgh.14498> (2019).
26. Ji, D. et al. Unreliable estimation of fibrosis regression during treatment by liver stiffness measurement in patients with chronic hepatitis B. *Am. J. Gastroenterol.* **116**, 1676–1685. <https://doi.org/10.14309/ajg.000000000001239> (2021).
27. Tai, D. C. et al. Fibro-C-Index: comprehensive, morphology-based quantification of liver fibrosis using second harmonic generation and two-photon microscopy. *J. Biomed. Opt.* **14**, 044013. <https://doi.org/10.1117/1.3183811> (2009).
28. Sun, Y. et al. New classification of liver biopsy assessment for fibrosis in chronic hepatitis B patients before and after treatment. *Hepatology* **65**, 1438–1450. <https://doi.org/10.1002/hep.29009> (2017).
29. Sun, Y. et al. Quantitative assessment of liver fibrosis (qFibrosis) reveals precise outcomes in Ishak stable patients on anti-HBV therapy. *Sci. Rep.* **8**, 2989. <https://doi.org/10.1038/s41598-018-21179-2> (2018).
30. Sun, Y. M. et al. Qualitative pathological assessment of liver fibrosis regression after antiviral therapy in patients with chronic hepatitis B. *Zhonghua Gan Zang Bing Za Zhi.* **25**, 819–826. <https://doi.org/10.3760/cma.j.issn.1007-3418.2017.11.005> (2017).
31. Wang, Y. et al. Systematic quantification of histological patterns shows accuracy in reflecting cirrhotic remodeling. *J. Gastroenterol. Hepatol.* **32**, 1631–1639. <https://doi.org/10.1111/jgh.13722> (2017).
32. Cabibi, D. et al. Comparison of histochemical staining methods and correlation with transient elastography in acute hepatitis. *Pathobiology* **82**, 48–52. <https://doi.org/10.1159/000375264> (2015).
33. Ishak, K. et al. Histological grading and staging of chronic hepatitis. *J. Hepatol.* **22**, 696–699. [https://doi.org/10.1016/0168-8278\(95\)80226-6](https://doi.org/10.1016/0168-8278(95)80226-6) (1995).
34. Bedossa, P. & Poynard, T. An algorithm for the grading of activity in chronic hepatitis C. The METAVIR Cooperative Study Group. *Hepatology* **24**, 289–293. <https://doi.org/10.1002/hep.510240201> (1996).
35. Kleiner, D. E. et al. Design and validation of a histological scoring system for nonalcoholic fatty liver disease. *Hepatology* **41**, 1313–1321. <https://doi.org/10.1002/hep.20701> (2005).
36. Bedossa, P. Reversibility of hepatitis B virus cirrhosis after therapy: who and why? *Liver Int.* **35**(Suppl 1), 78–81. <https://doi.org/10.1111/liv.12710> (2015).
37. Wanless, I. R., Bernier, V. & Seger, M. Intrahepatic portal vein sclerosis in patients without a history of liver disease. An autopsy study. *Am. J. Pathol.* **106**, 63–70 (1982).
38. Wanless, I. R., Nakashima, E. & Sherman, M. Regression of human cirrhosis. Morphologic features and the genesis of incomplete septal cirrhosis. *Arch. Pathol. Lab. Med.* **124**, 1599–1607. <https://doi.org/10.5858/2000-124-1599-rohc> (2000).
39. Hytioglou, P. & Theise, N. D. Regression of human cirrhosis: an update, 18 years after the pioneering article by Wanless et al. *Virchows Arch.* **473**, 15–22. <https://doi.org/10.1007/s00428-018-2340-2> (2018).
40. Rosmorduc, O. Antiangiogenic therapies in portal hypertension: a breakthrough in hepatology. *Gastroenterol. Clin. Biol.* **34**, 446–449. <https://doi.org/10.1016/j.gcb.2010.05.007> (2010).
41. Gao, J. et al. Angiocrine signaling in sinusoidal homeostasis and liver diseases. *J. Hepatol.* **81**, 543–561. <https://doi.org/10.1016/j.jhep.2024.05.014> (2024).
42. Jain, R. K. Antiangiogenesis strategies revisited: from starving tumors to alleviating hypoxia. *Cancer Cell.* **26**, 605–622. <https://doi.org/10.1016/j.ccell.2014.10.006> (2014).
43. Gill, R. M., Belt, P., Wilson, L., Bass, N. M. & Ferrell, L. D. Centrilobular arteries and microvessels in nonalcoholic steatohepatitis. *Am. J. Surg. Pathol.* **35**, 1400–1404. <https://doi.org/10.1097/PAS.0b013e3182254283> (2011).
44. Friedman, S. L. & Pinzani, M. Hepatic fibrosis 2022: unmet needs and a blueprint for the future. *Hepatology* **75**, 473–488. <https://doi.org/10.1002/hep.32285> (2022).
45. Liu, F. et al. qFIBS: an automated technique for quantitative evaluation of fibrosis, inflammation, ballooning, and steatosis in patients with nonalcoholic steatohepatitis. *Hepatology* **71**, 1953–1966. <https://doi.org/10.1002/hep.30986> (2020).
46. Glass, G., Papin, J. A. & Mandell, J. W. SIMPLE: a sequential immunoperoxidase labeling and erasing method. *J. Histochem. Cytochem.* **57**, 899–905. <https://doi.org/10.1369/jhc.2009.953612> (2009).
47. Lan, H. Y., Mu, W., Nikolic-Paterson, D. J. & Atkins, R. C. A novel, simple, reliable, and sensitive method for multiple immunoenzyme staining: use of microwave oven heating to block antibody crossreactivity and retrieve antigens. *J. Histochem. Cytochem.* **43**, 97–102. <https://doi.org/10.1177/43.1.7822770> (1995).
48. Wu, A. Y., Hong, T. H. & Rosenfeld, A. Threshold selection using quadrees. *IEEE Trans. Pattern Anal. Mach. Intell.* **4**, 90–94. <https://doi.org/10.1109/tpami.1982.4767203> (1982).
49. Krzywinski, M. & Altman, N. Classification and regression trees. *Nat. Methods.* **14**, 757–758. <https://doi.org/10.1038/nmeth.4370> (2017).

Author contributions

Z.X.L., Q.Y., Y.Y.R. and X.T. drafted the manuscript. Q.Y., Y.Y.R. and X.T. trained the algorithm. Z.X.L. collected samples and performed staining, analyzed and interpreted data. X.S. and Z.M.Z. revised the manuscript. D.C.S.T. and I.R.W. provided study supervision. J.M.S. engaged in critical revisions of the manuscript. C.H.L. conceived and designed the study. All authors read and approved the final manuscript.

Funding

National Natural Science Foundation of China (81730109, 82274305, 82305200, 82374122); National Science and Technology Major Project (2018ZX10302204); Shanghai Key Specialty of Traditional Chinese Clinical Medicine (shslczdk01201).

Declarations

Patient consent for publication

Written informed consent was obtained from all the participants prior to the enrollment of this study. To protect patient privacy, the pathology number serves as a unique identifier. The study have been performed in accordance with the Declaration of Helsinki. Approval Number: 2015-445-73-01, Institutional Review Board of Shuguang Hospital.

Competing interests

J.M.S. reports Consultant: Akero, Alentis Therapeutics, Astra Zeneca, Apollo Endosurgery, 89Bio, Boehringer Ingelheim, GSK, Ipsen, Inventiva Pharma, Madrigal, MSD, Northsea Therapeutics, Novartis, Novo Nordisk, Pfizer, Roche, Sanofi, Siemens Healthineers. Research Funding: Boehringer Ingelheim, Siemens Healthcare GmbH. Stock Options: AGED diagnostics, Hepta Bio. Speaker Honorarium: Gilead Sciences, Advanz, Echosens, MedPublico GmbH. The other authors do not have any disclosures to report.

Additional information

Supplementary Information The online version contains supplementary material available at <https://doi.org/10.1038/s41598-025-87427-4>.

Correspondence and requests for materials should be addressed to C.L.

Reprints and permissions information is available at www.nature.com/reprints.

Publisher's note Springer Nature remains neutral with regard to jurisdictional claims in published maps and institutional affiliations.

Open Access This article is licensed under a Creative Commons Attribution-NonCommercial-NoDerivatives 4.0 International License, which permits any non-commercial use, sharing, distribution and reproduction in any medium or format, as long as you give appropriate credit to the original author(s) and the source, provide a link to the Creative Commons licence, and indicate if you modified the licensed material. You do not have permission under this licence to share adapted material derived from this article or parts of it. The images or other third party material in this article are included in the article's Creative Commons licence, unless indicated otherwise in a credit line to the material. If material is not included in the article's Creative Commons licence and your intended use is not permitted by statutory regulation or exceeds the permitted use, you will need to obtain permission directly from the copyright holder. To view a copy of this licence, visit <http://creativecommons.org/licenses/by-nc-nd/4.0/>.

© The Author(s) 2025